



Mechanical and microstructural changes of skeletal muscle following immobilization and/or stroke

Naiim Jalal¹ · Jean-Michel Gracies^{1,2} · Mustapha Zidi¹

Received: 31 January 2019 / Accepted: 26 June 2019 / Published online: 6 July 2019
© Springer-Verlag GmbH Germany, part of Springer Nature 2019

Abstract

Patient management following a stroke currently represents a medical challenge. The presented study investigates the effect of immobilization on skeletal muscles in short positions after a stroke. A rat model was implemented in order to compare four situations within 14 days including control group, immobilization of one forelimb without stroke, stroke without immobilization and stroke with immobilization of the paretic forelimb. To analyze the changes of the mechanical properties of the passive skeletal muscle, the biological tissue is assumed to behave as a visco-hyperelastic and incompressible material characterized by the first-order Ogden's strain energy function coupled with second-order Maxwell's model. The material parameters were identified from inverse finite element method by using uniaxial relaxation tests data of skeletal muscle samples. Based on measurements of histological parameters, we observe that muscle immobilization led to microconstituents changes of skeletal muscles that were correlated with degradations of its mechanical properties. In the case of immobilization without stroke, the neurological behavior was also altered in the same manner as in the case of a stroke. We showed that immobilization of skeletal muscles in short positions produced contractile tissue atrophy, connective tissue thickening and alteration of passive mechanical behavior that were more damaging than the effects produced by a stroke. These results showed then that immobilization of skeletal muscles in short positions is highly deleterious with or without a stroke.

Keywords Skeletal muscle · Immobilization · Stroke · Visco-hyperelasticity · Collagen · Muscle fiber type

1 Introduction

After a stroke, a patient is placed in bed rest and some muscles of the patient are immobilized in a short position (Norvang et al. 2018). The disorder that we name “spastic myopathy post-stroke” might be considered as the consequences of a stroke and the immobilization in a short position that follow the stroke (Gracies 2015). Furthermore, it is well known that muscular damage might be a result of skeletal muscles in short positions. Indeed, immobilization in short positions is damaging to muscular tissue (Gracies 2005, 2015) and triggers a cascade of reactions inside the muscle.

Firstly, an early alteration of protein synthesis occurs in the first few hours, followed by non-contractile tissue thickening inducing loss of extensibility (Tabary et al. 1972; Booth et al. 2001; Hafer-Macko et al. 2008; Smith et al. 2011). In the case of post-stroke, it was therefore observed that the increase in skeletal muscle stiffness exacerbates the spasticity phenomenon that amplifies muscle immobilization in return. For these reasons, we assumed that this cycle of retraction–muscle hyperactivity–retraction maintains a real muscular disease that we will refer to as spastic myopathy (Gracies 2015). Nevertheless, tissue remodeling remains little known in this case and the significance of immobilization on the mechanical and structural properties of the tissue has yet to be quantified for post-stroke. Thus, it seems necessary to evaluate the deleterious impact of post-stroke immobilization knowing that few studies exist in human due to lack of data. For this reason, current research focuses on the development of animal models. Although both immobilization alone (Honda et al. 2018; Jones and Schallert 1994; Stevens et al. 1999; Tabary et al. 1972) and stroke alone (Longa et al. 1989; Ouk 2009; Parkkinen et al. 2013)

✉ Mustapha Zidi
zidi@u-pec.fr

¹ Bioengineering, Tissues and Neuroplasticity, EA 7377, Faculty of Medicine, Paris-East University at Créteil, 8 rue du Général Sarrail, 94010 Créteil, France

² Department of Neurolocomotion Therapy, Groupe Hospitalier Henri Mondor, Assistance Publique des Hôpitaux de Paris (AP-HP), Créteil, France

models are common in literature, there is almost no study that combines both pathologies. Furthermore, it should be emphasized that most of stroke model studies focused on pharmacological (Ouk et al. 2009; Desgeorges et al. 2017) or sensorimotor and cognitive purposes (Jones and Schallert 1994; Zhang et al. 2012; Zvejniece et al. 2012), but very few models focused on mechanical or structural properties of skeletal muscles (Abo et al. 2004). Previous researches have studied microstructural alteration of skeletal muscle in both immobilization alone (Tabary et al. 1972; Williams and Goldspink 1984; Stevens et al. 1999; Okita et al. 2004; Udaka et al. 2008; Honda et al. 2015, 2018) and stroke alone (Booth et al. 2001; Pontén and Stål 2007; Smith et al. 2011; de Bruin et al. 2014) cases, including, collagen content (Williams and Goldspink 1984; de Bruin et al. 2014; Honda et al. 2018), muscle typology (Stevens et al. 1999; Pontén and Stål 2007; Smith et al. 2011) or sarcomere length/number (Tabary et al. 1972; Williams and Goldspink 1984; de Bruin et al. 2014). Whole or sectioned healthy muscles have been studied experimentally to either tension (Calvo et al. 2010; Mohammadkhah et al. 2016; Wheatley et al. 2016a) and compression experiments (Böl et al. 2014; Jalal and Zidi 2018). The tissue mechanical properties were identified from these experiments using stress–stretch analytical expressions (Calvo et al. 2010; Wheatley et al. 2016a) or constitutive laws were implemented in finite element models (Bosboom et al. 2001; Chawla et al. 2009). We can note that some studies have taken into account the 3D realistic geometry of mechanically stimulated samples in their models (Böl et al. 2012; Gras et al. 2012). However, few studies have investigated the mechanical behavior of immobilized (Tabary et al. 1972; Williams and Goldspink 1984; Udaka et al. 2008; Honda et al. 2018) or paretic muscles (Smith et al. 2011; de Bruin et al. 2014) which are usually based on the comparison between healthy and diseased stress–stretch or length–tension curves.

Consequently, the following question is addressed: is immobilization of skeletal muscle in short position deleterious after stroke? An animal model will be implemented to investigate this question.

In this paper, we investigated this question from a new rat model combining ischemic stroke by transient middle cerebral artery occlusion (Longa et al. 1989) with immobilization of impaired limb (Jones and Schallert 1994). We evaluated three main metrics: first, infarct volume and neurological test; second, the microstructural composition of skeletal muscle, including collagen density, proportions of muscle fiber types and histomorphology of such fiber; third, the changes of the mechanical behavior of the passive skeletal muscle using a visco-hyperelastic (Holzapfel 1996) and incompressible material characterized by the first-order Ogden's strain energy function coupled with second-order Maxwell's model (Gras et al. 2013; Jalal and Zidi 2018).

The material parameters were identified from inverse finite element method by using uniaxial relaxation tests data of skeletal muscle samples. Measurements of histological parameters permitted to explain the mechanical and structural change of skeletal muscle subjected to immobilization and/or stroke.

2 Materials and methods

2.1 Animal model

Young adult Wistar rats of 8 weeks and 306 ± 22 g were obtained from Janvier Labs. Animal protocols were performed in accordance with the local ethics committee ANSES/ENVA/UPEC (n°13/12/16-10). The model implemented in the present study combined right cerebral artery occlusion with immobilization of the left forelimb on the chest during 14 days. Experiments were carried out in four groups of rats:

- Control (Cont), $N=7$
- Immobilization without stroke (Immo), $N=7$
- Stroke without immobilization (MCAo), $N=5$
- Stroke and immobilization (ImMCAo), $N=6$

2.1.1 Transient middle cerebral artery occlusion (MCAo)

Surgical procedures were carried out as previously described (Ouk et al. 2009). Briefly, a 4/0 monofilament nylon was placed through the carotid artery to plug the middle cerebral artery during 60 min. The control operation (for control and immobilized groups) required 60-min anesthesia and the same manipulations without advancing the monofilament until the obstruction. Further descriptions are given in “Appendix” (Fig. 7a, b).

2.1.2 Immobilization

The immobilization protocol was implemented on the left forelimb during the 60-min anesthesia of MCAo procedure. First, digits were fixed in flexed position by using scotch tape. Then, the ipsilateral forelimb was huddled up against the chest with the wrist in a palmar flexed position through the use of plaster cast (Biplatrix®, BSN medical). Plaster thus constitutes a one hole vest where the forelimb could do only limited movements (Fig. 7c) (Jones and Schallert 1994).

2.2 Sample conditioning

Rats were killed on the fourteenth day with an overdose of pentobarbital. Brains, as well as biceps brachii (long head)

and flexor carpi ulnaris muscles, were harvested. The superficial connective tissue of both muscles, aponeurosis and epimysium, was carefully dissected during the harvesting process. Brains were frozen in isopentane at $-20\text{ }^{\circ}\text{C}$ during 30 min and then stored in aluminum at this same temperature until cutting. The long head of biceps brachii muscles was stored in NaCl 0.9% (B. Braun, Melsungen, Germany) at $4\text{ }^{\circ}\text{C}$ until the tensile test. Lastly, flexor carpi ulnaris muscles were divided into two parts. The proximal part was snap-frozen in isopentane cooled in liquid nitrogen (Honda et al. 2018), whereas the distal part was embedded in paraffin.

2.3 Brain infarct volume measurement

First, $50\text{ }\mu\text{m}$ coronal slices were cut on a cryostat (CM3050 S, Leica Biosystems GmbH, Nussloch, Germany) at $-20\text{ }^{\circ}\text{C}$ and dropped off on slides (SuperFrost Plus™, Thermo Fisher Scientific, Waltham, MA). Slides were made at 12 levels in roughly 1 mm steps identified in the Paxinos & Watson stereotaxic atlas. Then, slides were stained using a Cresyl Violet protocol previously described (Ouk et al. 2009). Infarcted part, with a reduced cellular density, appears brightest. Finally, the infarcted volume was obtained by integrating surface density S_i measured using ImageJ software (NIH), $V_I = \sum_{i=1}^{12} S_i \cdot d_i$, where V_I was the estimated volume and d_i is the distance between two slides that was set to 1 mm. The corrected infarct volume $V_{I_c} = V_I \cdot V_{HH}/V_{HD}$ reflecting the cerebral edema was determined from the healthy V_{HH} and damaged hemisphere V_{HD} .

2.4 Microstructural characterization

The distal parts of flexor carpi ulnaris muscles were embedded in paraffin and cut into $4\text{ }\mu\text{m}$ slices. Sections were stained in Sirius red (0.1% solution of picosirius red F3BA in a saturated solution of acid picric) as previously described (Junqueira et al. 1979).

Histochemical and immunofluorescence staining was performed. Slides were scanned with Lamina Scanner (Perkin Elmer, Waltham) and viewed using CaseViewer 2.2 software (3D HISTECH Ltd).

2.4.1 Collagen analysis

As others microconstituents, collagen of perimysium and endomysium was obtained by a semiautomatic interface developed in MATLAB 2017b (MathWorks, Natick, Ma). Briefly, as the collagen in perimysium was more colored than collagen in endomysium, a k -mean clustering algorithm allowed differentiating those two connective tissues. Refer to “Appendix” (Fig. 8) for further description. Misallocations of certain parts due to chromatic aberration could be corrected by the user. Epimysium was not quantified since it

was almost entirely removed during dissection. The remaining epimysium was deducted to perimysium area. Furthermore, tendinous arch, which connected humeral and ulnar head, were independently quantified. Surface densities $\rho_T = S_T/S_{\text{Total}}$ (T = endomysium, perimysium, tendinous arch) were then calculated by dividing the collagen area by the muscle cross-sectional area S_{Total} that was computed from the total tissue slice area where the empty regions that appeared white were subtracted from the total area calculation (Schipke et al. 2017). White empty spaces were artifacts due to histochemical protocol and were removed using a luminance threshold in CIELAB color space.

2.4.2 Histomorphology

Fiber morphological analysis was performed using a customized labeling interface developed using MATLAB. This interface included filtering tools in CIELAB color space and mathematical morphology tools. If necessary, the user could manually count bonded fibers by allocating the real number of fibers. The mean (E_a) \pm standard deviation (S_a) values for the fiber area were determined using the described procedure. The normalized standard deviation $S_a^n = S_a/E_a$ measured the size variations.

Furthermore, for each fiber, isoperimetric quotients, denoted $Q = 4\pi a/p^2$, were obtained in which a represents the fiber area and p its perimeter. This coefficient gives circularity information, since $Q = 1$ in the case of a circle and $Q < 1$ otherwise. The mean (E_Q) and the normalized standard deviation (S_Q^n) values were then calculated.

2.4.3 Immunohistology

The slides were produced from proximal parts of the flexor carpi ulnaris using primaries antibodies to slow myosin heavy chain isoform (MHCI) and to one fast myosin heavy chain isoform (MHCII_a) (Bloemberg and Quadrilatero 2012).

2.4.4 MHC analysis

Type I, type II_a and hybrid I/II_a fibers were quantified by a semiautomatic interface developed in MATLAB. The fibers were manually pointed by the user with a square region of interest (ROI) inside the fiber. A mean green and blue fluorescence wavelengths were recorded inside the ROI of each fiber. The green and blue average wavelengths corresponded, respectively, to the proportion of MHCI and MHCII_a isoform expressed by fibers. Then, a custom k -mean clustering algorithm quantized type I, type II_a and hybrid fibers. Finally, the area densities f_I , f_{II_a} and f_{I-II_a} were computed from total surface area. Refer to “Appendix” (Fig. 9) for further description.

2.5 Passive mechanical behavior of skeletal muscle

Long head of biceps brachii muscles was extracted immediately after killing the animals. The muscles were stored in NaCl 0.9% (B. Braun, Melsungen, Germany) at 4 °C until tensile test achieved at room temperature. The experiments were carried out between 1- and 2-h postmortems in order to avoid, on the one hand, the spontaneous rhythmic contraction immediately following extraction (Honda et al. 2018), on the other hand, the rigor mortis phenomenon (Van Loocke et al. 2006). Note that the humid mass was weighed before the test. Relaxation tests were performed by the uniaxial mechanical testing system (MTS Insight, MTS Systems Corporation, Eden Prairie, Mn). The test machine was controlled by data processing software (TestWorks.5, MTS Systems Corporation, Eden Prairie, Mn). Tendons were fully secured in jaws, and sandpaper pieces were added between muscles and jaws in order to avoid any slippage (Calvo et al. 2010).

A 0.1 N preload was applied in order to stabilize the mechanical behavior (Mohammadkhah et al. 2016). A loading was then imposed at a strain rate of 0.5% s⁻¹ up to 10% strain. Then, the strain was kept constant for 300 s to allow stress relaxation in the sample. Finally, the muscles were unloaded until 0.1 N and stretched again at the same strain rate up to any signs of slippage. Forces over time were recorded by a 100 N force sensor and smoothed in MATLAB.

On the other hand, 3D reconstructions of muscles were completed by using 2 cameras (Hero 5 Black edition) and a custom reconstruction algorithm.

2.5.1 Constitutive law

The mechanical behavior of the passive skeletal muscle was assumed to be made of a visco-hyperelastic and nearly incompressible (Holzapfel 1996). Hyperelastic behavior was described by first-order Ogden model (Ghoreishy 2012; Jalal and Zidi 2018) strain energy:

$$W = w(\mathbf{C}) + U(J), \quad (1)$$

with $w(\mathbf{C})$ and $U(J)$ are the isochoric and purely volumetric contribution of W defined by:

$$w = \frac{\mu}{\alpha} (\lambda_1^\alpha + \lambda_2^\alpha + \lambda_3^\alpha - 3), \quad (2)$$

and

$$U = \frac{1}{D} (J - 1); \quad (3)$$

here \mathbf{C} denotes the right Cauchy–Green tensor, $J = \lambda_1 \lambda_2 \lambda_3$ denotes the determinant of deformation gradient tensor where λ_i ($i = 1, 2, 3$) are the principal stretches, μ is the shear modulus. α is a dimensionless curvature parameter. Furthermore, the time function describing the viscoelastic

behavior is represented by the Prony series (Holzapfel 1996; Van Loocke et al. 2008):

$$\gamma(t) = \gamma_\infty + \sum_{k=1}^n \gamma_k e^{-\frac{t}{\tau_k}}, \quad (4)$$

where τ_k are the relaxation times, γ_∞ and γ_k are the relative moduli for branches of Maxwell's model. Each γ_k is defined as follows:

$$\gamma_k = E_k / \left(E_\infty + \sum_{k=1}^n E_k \right), \quad \gamma_\infty = E_\infty / \left(E_\infty + \sum_{k=1}^n E_k \right) \quad (5)$$

where E_k is the elastic modulus of the k th spring and E_∞ is the modulus of the infinite lone spring. Therefore, γ_k is related to γ_∞ as $\gamma_\infty + \sum_{k=1}^n \gamma_k = 1$.

To limit the number of material parameters necessary in the model, we assume that the mechanical response of the skeletal muscle is described by only two branches of Maxwell's model. In this case, if we consider the only isochoric contribution, the constitutive equation law is given as follows (Holzapfel 1996):

$$S = \int_0^t \left[\gamma_\infty + \gamma_1 e^{-\frac{t-\tau}{\tau_1}} + \gamma_2 e^{-\frac{t-\tau}{\tau_2}} \right] \left(2 \frac{d}{d\tau} \frac{dw}{d\mathbf{C}} \right) d\tau, \quad (6)$$

where S is the second Piola–Kirchoff stress tensor.

Finally, the Young's modulus $E_0 = 3\mu\alpha/2$ of the hyperelastic branch and the total relaxation ratio $\gamma_T = \gamma_1 + \gamma_2$ were computed.

2.5.2 Inverse finite element model

Tensile relaxation tests were modeled with a finite element method using ANSYS Mechanical APDL 17.2 (ANSYS Inc., Canonsburg). The real sample geometries included by importing the 3D reconstruction of the tissue using MATLAB. For the simulations, an average of 582 quadratic tetrahedral elements (SOLID 187 with 10 nodes) and 1127 nodes were implemented. The mesh size was chosen after a mesh sensibility study had been performed in order to choose the coarser mesh with good relevance. The displacement boundary conditions were prescribed on top surface, while fixing displacement in orthogonal directions and the bottom surfaces were fixed. The visco-hyperelastic model was chosen as previously described with material parameters to optimize the parameter vector $\mathbf{V}_p^{opt} = [\mu, \alpha, \tau_i, \gamma_i; (i = 1, 2)]$ (Fig. 10). Note that D is fixed at 10^{-3} since skeletal muscle is considered nearly incompressible (Böl et al. 2014).

Table 1 Initial material parameters' values of inverse finite element method

Parameters	μ (kPa)	α	γ_1	τ_1 (s)	γ_2	τ_2 (s)
Boundaries	[1; 2000]	[0.1; 100]	[0.1; 0.9]	[0.1; 50]	[0.1; 0.9]	[50; 1000]
Initial value	50	3.5	0.5	5	0.3	80

2.5.3 Material parameters' identification

The vector V_p^{op} was identified by an inverse finite element method. For that, numerical reaction forces over time $F_z^n(t_i, V_p)$ were fitted with experimental reaction forces $F_z^e(t_i)$ in order to minimize the following objective function:

$$\varepsilon = \sum_{i=1}^m [F_z^n(t_i, V_p) - F_z^e(t_i)]^2, \quad (7)$$

where m is the number of measuring points and t_i time during the test. The objective function was minimized using the Levenberg–Marquardt algorithm included in lsqnonlin MATLAB function. Furthermore, the coefficients of determination were determined in order to evaluate fitting quality. Note that the initial parameters (Table 1) were fixed from the analytical value obtained in a preliminary study (Jalal and Zidi 2018).

It must be emphasized that algorithm convergence was verified by analyzing re-convergence of optimized parameters and by disrupting initial parameters.

2.6 Statistics

A two-way ANOVA with immobilization and stroke as factors was performed, including the interactions of the factors. Then, a Tukey–Kramer post hoc test was achieved. All statistical processing was implemented in MATLAB by setting the significance threshold $p = 0.05$. The statistical model validity was verified by testing residuals normality, independence and homogeneity of the variance.

3 Results

3.1 Infarct volume measurement: groups distribution

The mean total hemispheric volume is $619 \pm 50 \text{ mm}^3$, and infarcted areas range from 16 to 321 mm^3 . Some lesions that were located exclusively in the subcortical zone persisted, whereas some lesions recovered in cortical and subcortical areas. Only rats that had lesions larger than 50 mm^3 were included in MCAo and ImMCAo groups. They exhibited mean a volume lesion of $182 \pm 81 \text{ mm}^2$ [$50 - 321 \text{ mm}^2$] including, in any case, putamen and internal and external capsules that have been reported as most common affected cerebral areas in case of post-stroke spastic paresis (Picelli et al. 2014; Cheung

et al. 2016). Rats with lesions smaller than 50 mm^3 were excluded from the study.

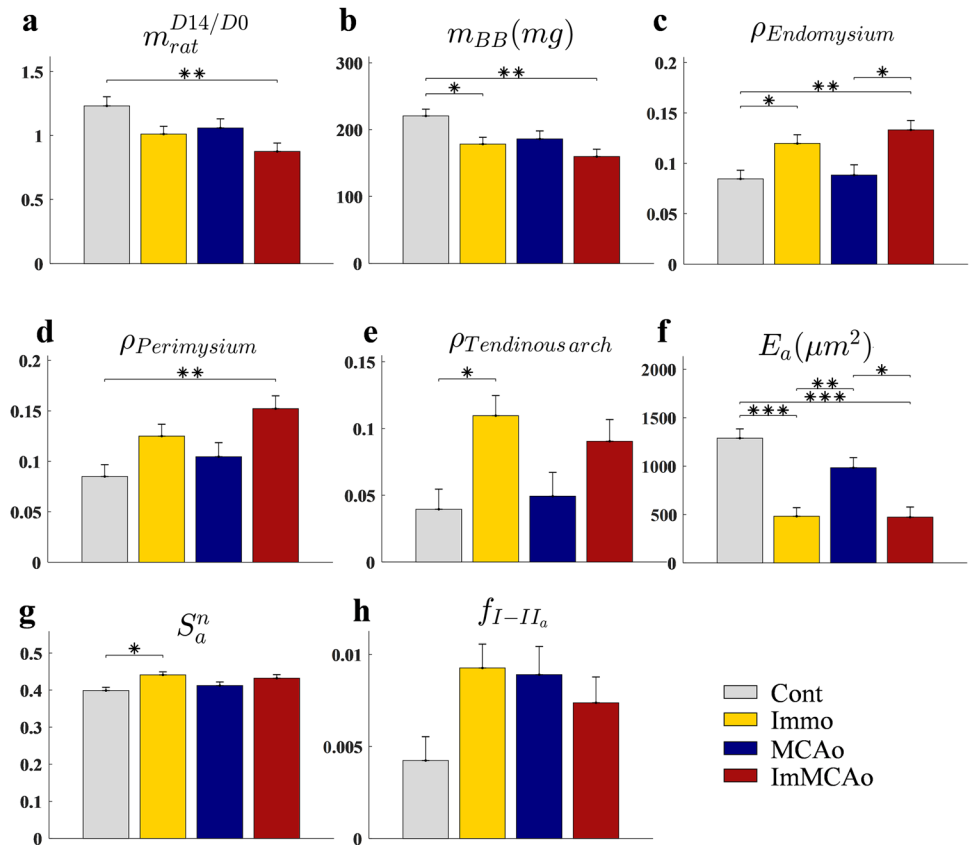
3.2 Body and muscle wet weight

Histograms of body weight between D_0 and D_{14} as well as biceps brachii wet weight are shown in Fig. 1a–b. Body weights of control rat increased by 23% within 14 days, whereas rats of Immo and MCAo group showed little weight gain (1% and 6%, respectively). Rats of ImMCAo group lose an average of 12% of their weight at D_{14} . Left biceps brachii wet weight followed the same variations as body weight. When considered independently, immobilization and stroke affected significantly both body weight ($p_{\text{Im}} = 0.008$ and $p_{\text{AVC}} = 0.034$) and left biceps brachii wet weight ($p_{\text{Im}} = 0.005$ and $p_{\text{AVC}} = 0.024$). Finally, correlation between both mass and Infarct volumes has been computed; refer to the “Appendix” section (Fig. 11a–b) for further description.

3.3 Collagen densities

Histograms of collagen surface densities of endomysium, perimysium and tendinous arch are presented in Fig. 1c–e. Endomysium ($\rho_{\text{Endomysium}}$) and perimysium ($\rho_{\text{Perimysium}}$) surface densities progressed from $\rho_{\text{Endomysium}}^{\text{Cont}} = 8.4\%$, $\rho_{\text{Perimysium}}^{\text{Cont}} = 8.5\%$ for the control group to $\rho_{\text{Endomysium}}^{\text{Im}} = 12\%$, $\rho_{\text{Perimysium}}^{\text{Im}} = 12.5\%$ and $\rho_{\text{Endomysium}}^{\text{AVCI}} = 13.3\%$, $\rho_{\text{Perimysium}}^{\text{AVCI}} = 15.2\%$ for the Immo and ImMCAo groups ($p_{\text{Im/Cont}}^{\text{Endo}} = 0.043$; $p_{\text{AVCI/Cont}}^{\text{Endo}} = 0.005$ and $p_{\text{Im/Cont}}^{\text{Peri}} = 0.108$; $p_{\text{AVCI/Cont}}^{\text{Peri}} = 0.004$). As other connective tissue, tendinous arch ($\rho_{\text{Tendinous arch}}$) dramatically increased for both immobilized groups from $\rho_{\text{Tendinous arch}}^{\text{Cont}} = 3.9\%$ to $\rho_{\text{Tendinous arch}}^{\text{Im}} = 11\%$ and $\rho_{\text{Tendinous arch}}^{\text{AVCI}} = 9\%$ for Immo and ImMCAo groups ($p_{\text{Im/Cont}}^{\text{Tend}} = 0.017$ and $p_{\text{AVCI/Cont}}^{\text{Tend}} = 0.13$). We note that the collagen surface densities in endomysium and perimysium were greater in the ImMCAo group than in the Immo group ($p_{\text{AVCI/AVC}}^{\text{Endo}} = 0.020$; $p_{\text{AVCI/AVC}}^{\text{Peri}} = 0.085$). Finally, when considered independently, immobilization factor was significant for all conjunctive tissues ($p_{\text{Im}}^{\text{Endo}} = 3e^{-4}$; $p_{\text{Im}}^{\text{Peri}} = 0.002$ and $p_{\text{Im}}^{\text{Tend}} = 0.001$). On the contrary MCAo factor just trend toward significance for collagen density in perimysium ($p_{\text{AVC}}^{\text{Peri}} = 0.077$). The conjunctive tissue thickening is represented in Fig. 2 by the blue and black arrow for endomysium and perimysium, respectively, and tendinous arches are indicated by a green star. Collagen surface density of tendinous arch was 2.8 and

Fig. 1 Histogram and correlation of some parameters between groups. **a** Body weight change between D_0 and D_{14} ($m_{rat}^{D14/D0}$). **b** Biceps brachii wet weight at D_{14} (m_{BB}). **c–e** Collagen surface densities in endomysium ($\rho_{endomysium}$), perimysium ($\rho_{perimysium}$) and tendinous arch ($\rho_{tendinous\ arch}$), respectively. **f, g** Mean (E_a) and normalized standard deviation (S_a^n) of fibers area. **h** Area density of hybrid muscle fiber I–II_a



2.3 higher in Immo and ImMCAo groups in comparison with rats of the control group.

3.4 Histomorphology

Mean muscle fiber area was significantly smaller in immobilized groups than in the control group ($p_{Im/Cont} = 4e^{-5}$ and $p_{AVCI/Cont} = 8e^{-5}$) (Fig. 1f). This atrophy is particularly noticeable in Fig. 2f in comparison with rats of the control group in Fig. 2c. We observe that the mean muscle fiber area of MCAo group was reduced by 24% with respect to control group ($p_{AVC/Cont} = 0.176$) but was significantly higher than the immobilized group. Atrophy came with an increase in the variability of fiber area ($p_{Im/Cont} = 0.012$ and $p_{AVCI/Cont} = 0.085$) (Fig. 1g). We can note an increased variability of fiber area for an immobilized rat (Fig. 2f) in relation to rats of the control group (Fig. 2c). When considered independently, the immobilization factor was significant for both measures ($p_{Im}^{Moy} = 2e^{-6}$ and $p_{Im}^{E-T} = 0.003$). On the contrary, MCAo factor seemed to have little impact on fiber size in the short term ($p_{AVC}^{Moy} = 0.129$ and $p_{AVC}^{E-T} = 0.808$). Finally, no differences were observed in the isoperimetric quotient between groups.

3.5 Muscle fiber type

Few differences in muscle fiber ratio were found between groups. Nevertheless, the surface ratio of hybrid fibers of type I – II_a increases nonsignificantly in Immo, MCAo and ImMCAo groups with respect to control group ($p_{Im/Cont} = 0.055$; $p_{AVC/Cont} = 0.125$ and $p_{AVCI/Cont} = 0.377$) (Fig. 1h). Hybrid fibers are marked with an orange star in Fig. 3 for one representative rats of the control group and one of ImMCAo group.

3.6 Mechanical parameters identification

Uniaxial relaxation traction tests have been performed on different samples obtained from each group. An illustrative profile of force versus displacement for the loading path and force versus time for the relaxation phase is shown for each group (Fig. 4a, b).

The best fit values of the material parameters' vector V_p^{op} were computed by an inverse finite element method by using tensile relaxation tests. Hyperelastic parameters are given in Fig. 5. Note that there were no statistical differences between groups for all parameters. However, we can show that the shear modulus increased in the immobilized group and the curvature parameter was lower in those groups, which means that immobilization in short position could

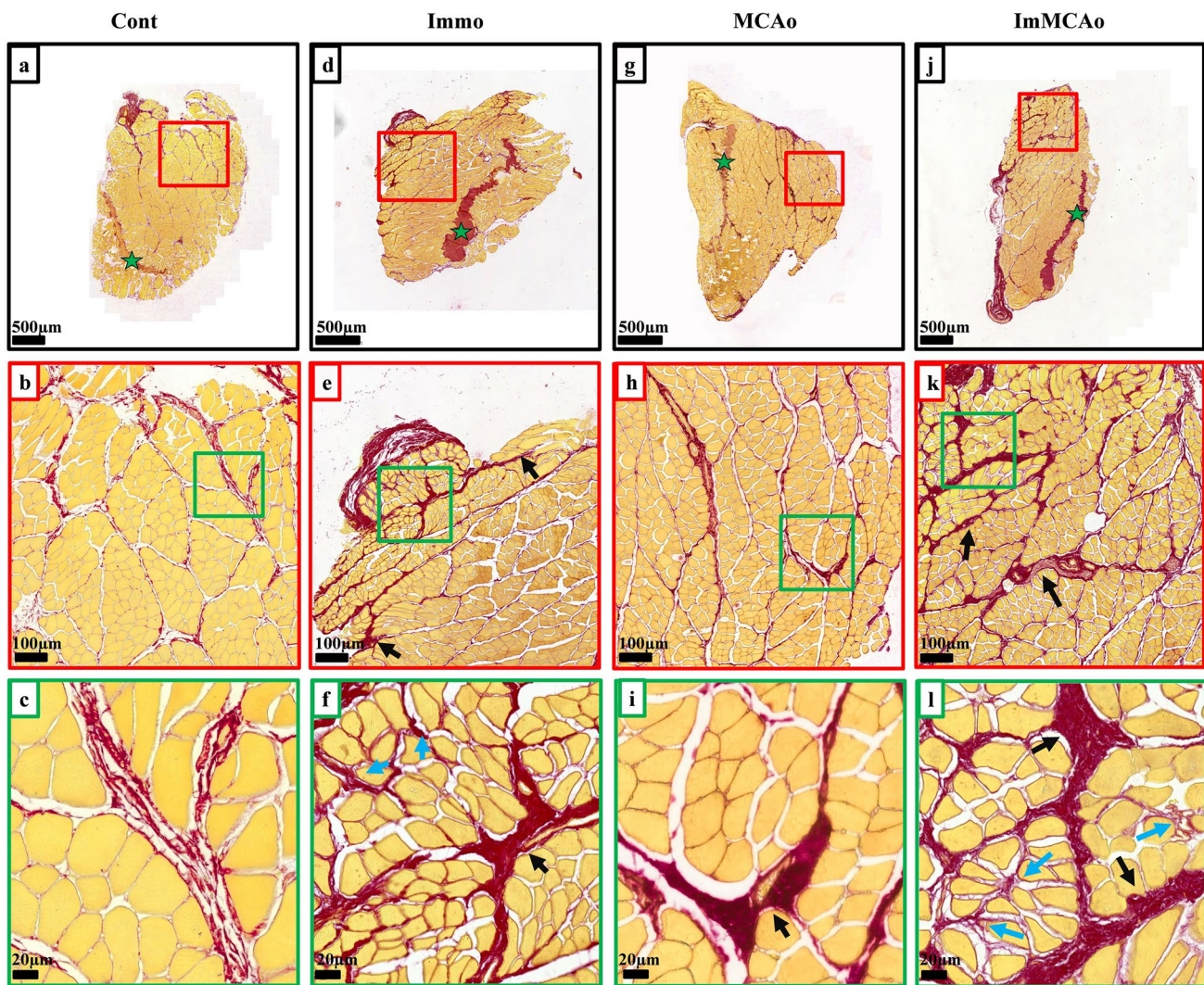


Fig. 2 Collagen in FCU slice with Sirius red staining. Rat of group **a–c** control, **d–f** immobilization, **g–i** MCAo, **j–l**, MCAo followed by immobilization of paretic immobilization. Green stars show tendi-

nous arch, and blue and black arrows point to thick endomysium and perimysium, respectively

lead to stiffening and a loss of nonlinearity of the immobilized muscle. Furthermore, when considered independently, the immobilization factor had an impact on total relaxation ratio ($p_{lm}^{\gamma_T} = 0.055$).

3.7 Correlation

Correlations between the mechanical parameters μ , α , E_0 , γ_T and the collagen densities are presented in Fig. 6. Pearson coefficients, as well as p value, are listed in Table 2. It must be emphasized that totally the collagen densities ρ_{Collagen} included endomysium and perimysium collagen but not the collagen located in the tendinous arch. Correlations were made on all rats but also for non-immobilized (Cont and MCAo) and immobilized (Immo and ImMCAo) groups taken independently. Instantaneous Young's modulus E_0

and shear modulus μ were significantly correlated with collagen density of endomysium ($r^{E_0} = 0.412$; $p^{E_0} = 0.041$ and $r^\mu = 0.446$; $p^\mu = 0.025$) and almost significantly correlated with the total collagen ($r^{E_0} = 0.347$; $p^{E_0} = 0.089$ and ($r^\mu = 0.348$; $p^\mu = 0.088$). In addition, we can notice a nonsignificant negative trend between dimensionless curvature α parameter and endomysium collagen density ($r^\alpha = -0.291$; $p^\alpha = 0.158$). Lastly, the total relaxation ratio γ_T was almost positively correlated with the endomysium ($r^{\gamma_T} = 0.394$; $p^{\gamma_T} = 0.052$) and the total collagen densities ($r^{\gamma_T} = 0.360$; $p^{\gamma_T} = 0.077$). Moreover, when considered independently, the immobilized and non-immobilized groups were most of the time similarly correlated to the global tendencies although not significantly. It is noticed that correlation between collagen densities in perimysium and the mechanical parameters follows the same trend than for the

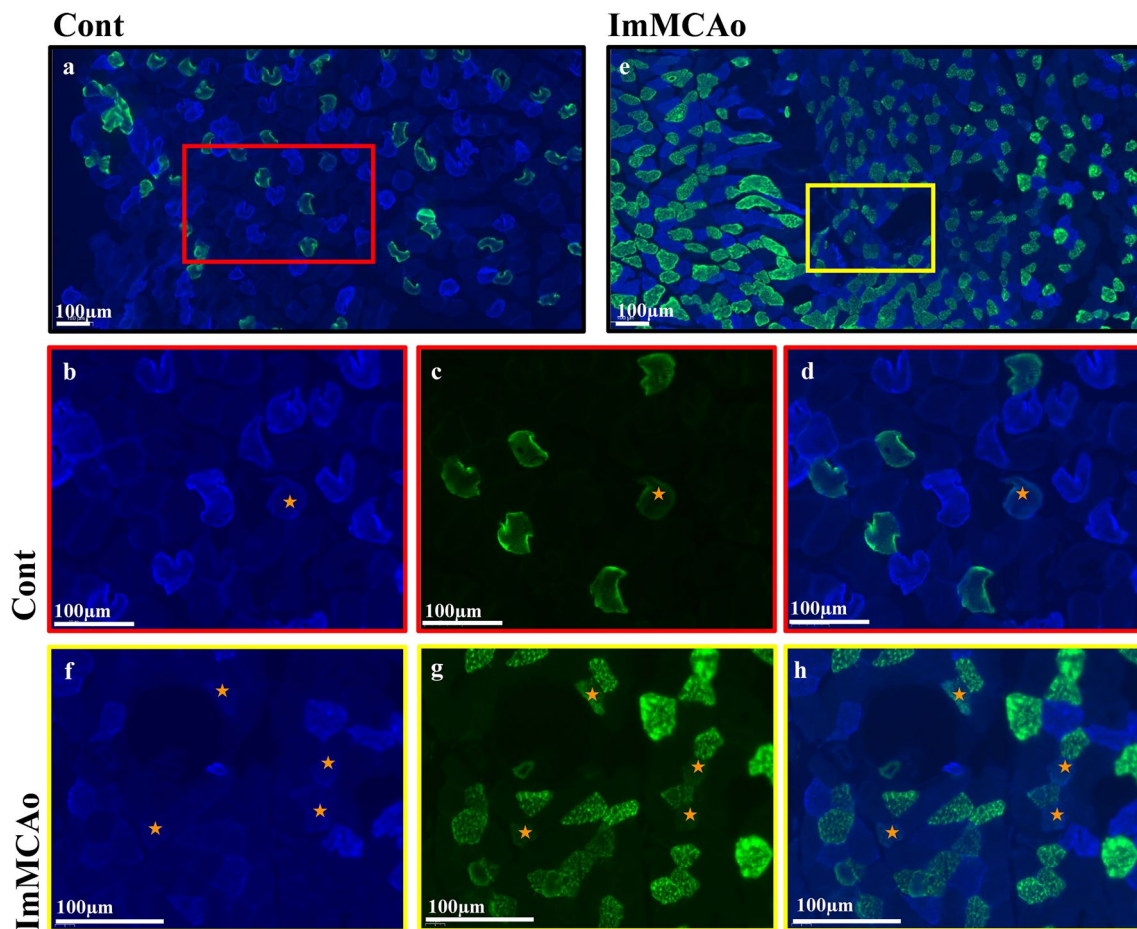


Fig. 3 Representative images of rat FCU slice showing type I (green), II_a (blue) and hybrid I/II_a (orange stars) fibers in case of control (cont) and stroke followed by immobilization (ImMCAo)

endomysium/total collagen densities (although not significantly). Thus, the higher the collagen densities, particularly in endomysium, the stiffer and higher linear the mechanical behavior and the more stress relaxed during relaxation phase.

4 Discussion

4.1 Brain infarct volume

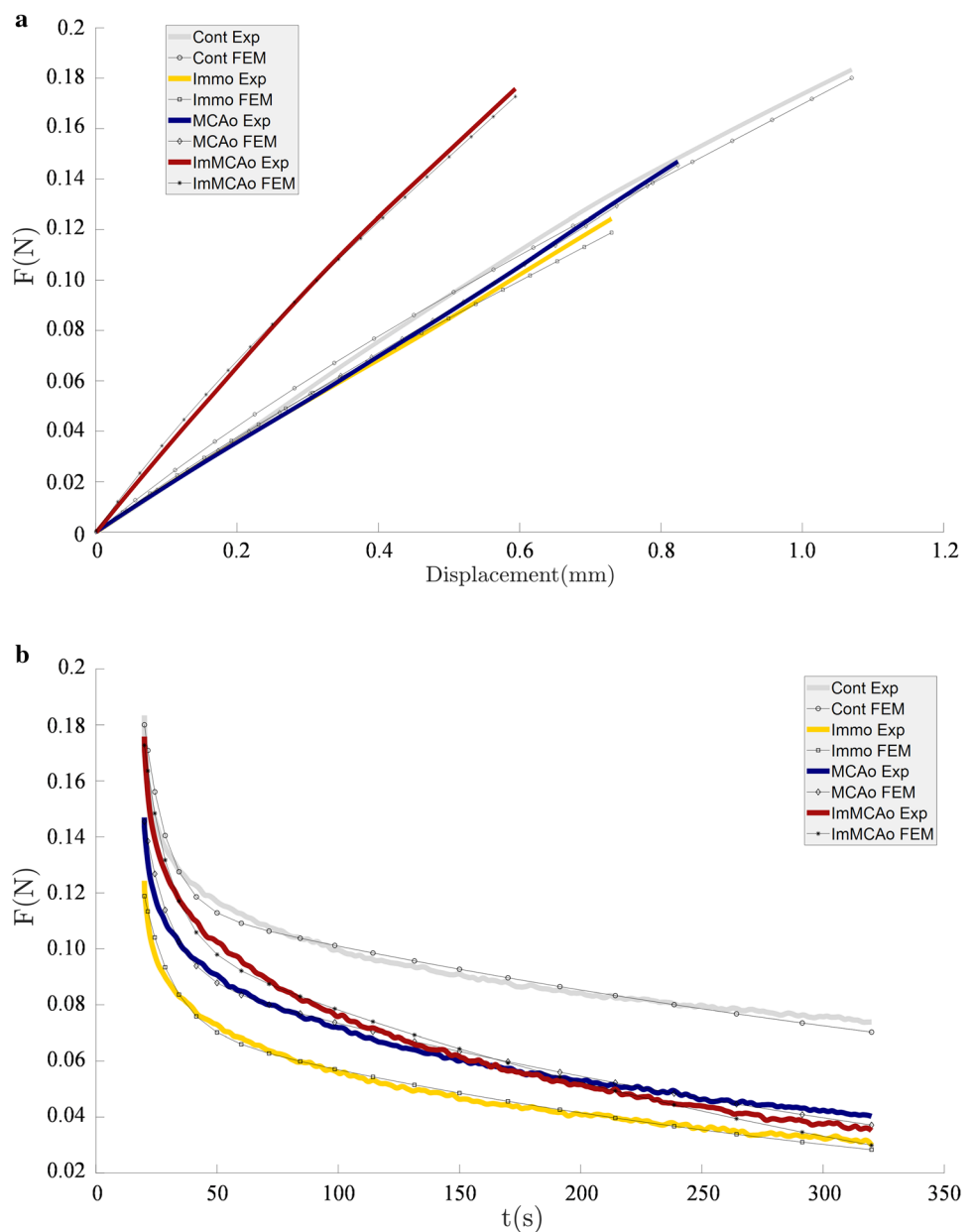
The mortality rate (32.1%) was comparable to a previous meta-analysis that showed mortality was $15.1 \pm 13.5\%$ [0% to 60.4%]. We note that the number of the rat of all groups reduced. This was particularly true for both MCAo and ImMCAo groups with, respectively, 5 and 6 animals. However, it should be underlined that numerous studies in our scope of work used groups of similar size (Stevens et al. 1999; Coq and Xerri 1999; Shortland et al. 2002; Bouley et al. 2007; Pontén and Stål 2007; Wheatley et al. 2016b). This small size was due to the infarct size exclusion criteria of 50 mm^3 . Indeed, in the present study, we chose to

include animals that had at least subcortical lesion larger than 50 mm^3 . All the lesions have affected putamen, internal capsule and external capsule that have been reported as the worst affected area in spastic paresis patient (Picelli et al. 2014; Cheung et al. 2016). The average size of the infarcted area was $182 \pm 81 \text{ mm}^2$, which is comparable to the previous study on rat of the same age. These were included between 120 mm^2 (Liu et al. 2016; Rogers et al. 1997), $243 \pm 16 \text{ mm}^2$ (Gautier et al. 2009) and $282 \pm 8 \text{ mm}^2$ (Ouk et al. 2009).

4.2 Body and muscle mass

At the overall level, we noted an increase in body mass of 23% for the control group during the first 14 days, whereas Immo and MCAo groups had little body mass change during this period (Fig. 1a). It must be emphasized that these results were in agreement with studies from the literature (Li et al. 2011; Parkkinen et al. 2013; Desgeorges et al. 2017). A study on cerebral palsy following injury of the spinal cord (Strata et al. 2004) showed that rats of immobilized groups are 30 to 45% lighter than control rats after

Fig. 4 Illustrative example of tensile relaxation test of skeletal muscle for all groups: Cont, Immo, MCAo, ImMCAo. **a** The load–displacement curves illustrate the loading path. **b** The load–times curves illustrate the relaxation



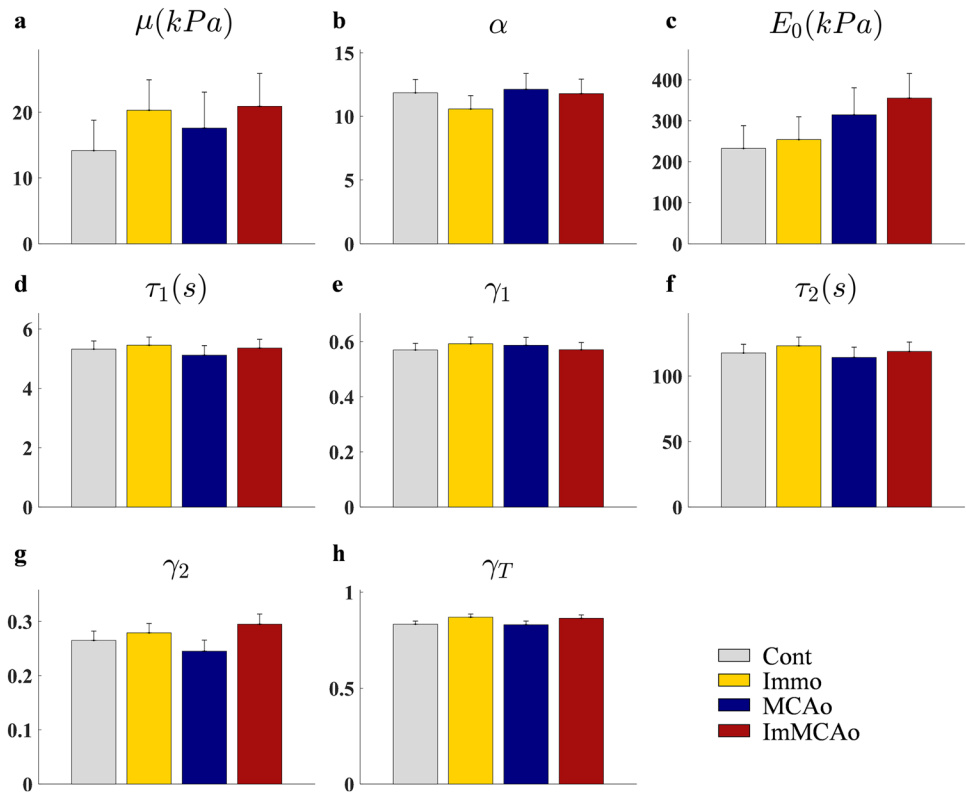
17 days of immobilization. In addition, in conformity with the mass loss (12%) of ImMCAo group in our study, Strata et al. (2004) showed that rats subjected to both immobilization and spinal cord injury were the lighter. Furthermore, BB mass loss of immobilized groups (Fig. 1b) was in agreement with previous studies on soleus muscles subjected to 2 to 6 months of immobilization (Honda et al. 2018; Spector et al. 1982; Stevens et al. 1999; Udaka et al. 2008).

4.3 Connective tissue

At the microstructural level, we note that immobilization produced an increase in collagen surface densities in both endomysium (Fig. 1c) and perimysium (Fig. 1d). These

increases of 40 to 80% with respect to control group are in accordance with data of the literature on rats immobilization (Honda et al. 2018) and on patients with spastic paresis (Smith et al. 2011). We quantified tendinous arch collagen densities (Fig. 1e), which constituted a new data to the author knowledge. As for endomysium and perimysium, this collagen density increases in both immobilized groups. Otherwise, it should be emphasized that the total collagen density of control group ($\rho_{\text{Collagen}} = 0.17$) was consistent with a previous study on others healthy muscles (Smith and Barton 2014). In addition, changes of collagen density in FCU endomysium of our study were similar to those obtained on human FCU that increased from 0.07 for control to 0.1 for the spastic patient (de Bruin et al. 2014).

Fig. 5 Histogram of biceps brachii visco-hyperelastic parameters between groups. Material parameters' vector was computed by an inverse finite element method (FEM)



We showed that rats of group MCAo were not exhibiting an increase in collagen density in endomysium and solely and a nonsignificant slight increase in perimysium. Thus, results from Immobilized groups were closer of what is observed in patients with spastic paresis.

4.4 Myofiber size

Along with the fibrosis, we note that mean muscle fibers cross-sectional area decreased dramatically for the immobilized group (Fig. 1f). This 60% decrease was comparable with another study on rat immobilized soleus (Honda et al. 2015), and with the study on spastic paresis patients (Smith et al. 2011; de Bruin et al. 2014) with, respectively, 45, 60 and 27% of fiber cross-sectional area decreases with respect to control group. Rats of the immobilized group had significantly smaller fiber cross-sectional area than the rats of MCAo group. Furthermore, the variability of muscle fiber cross-sectional area increases significantly (Fig. 1g) due to immobilization, which is in agreement with results obtained qualitatively on patients with spastic paresis (Booth et al. 2001; Pontén et al. 2007; Zogby et al. 2017). Thus, we showed that immobilization affects significantly transversal morphology that leads to morphological characteristics close to that observed on spastic paretic patients. Otherwise, it was noticed muscle fiber of patients with spastic paretic had a transversal geometry

more circular than healthy subjects (Booth et al. 2001). We proposed an index of circularity to measure this phenomenon. Nevertheless, we found no significant differences between groups. It should be underlined that the circular form of pathological muscle fiber remains qualitative and may vary among patients (Booth et al. 2001).

4.5 Myofiber typing

Skeletal muscle can adapt its myofiber typology in response to the functional demands (Leeuw and Pette 1996). For this reason, we measured the proportions of some muscle fiber types. The area densities f_I and f_{II_a} of muscle fiber of type I and II_a did not differ between groups. It should be noted that studies on spastic paresis patient do not lead to a consensus concerning muscle typology. Thus, studies in the literature showed that the proportion of fast fiber increased (De Deyne et al. 2004; Pontén and Stål 2007), while some studies showed that the proportion of these types of fibers decreased (Smith et al. 2011). In particular, De Bruin et al. (2014) showed that muscle typology of patients with spastic paresis did not differ from control tissues. Studies on immobilized rats showed a change of muscle typology with an increase in fast fiber Booth and Kelso 1973; Udaka et al. 2008). However, these modifications were quantified at 4-week immobilization. In the light of the long myosin heavy chain half-life of 13 days (Leeuw and Pette 1996), it was not

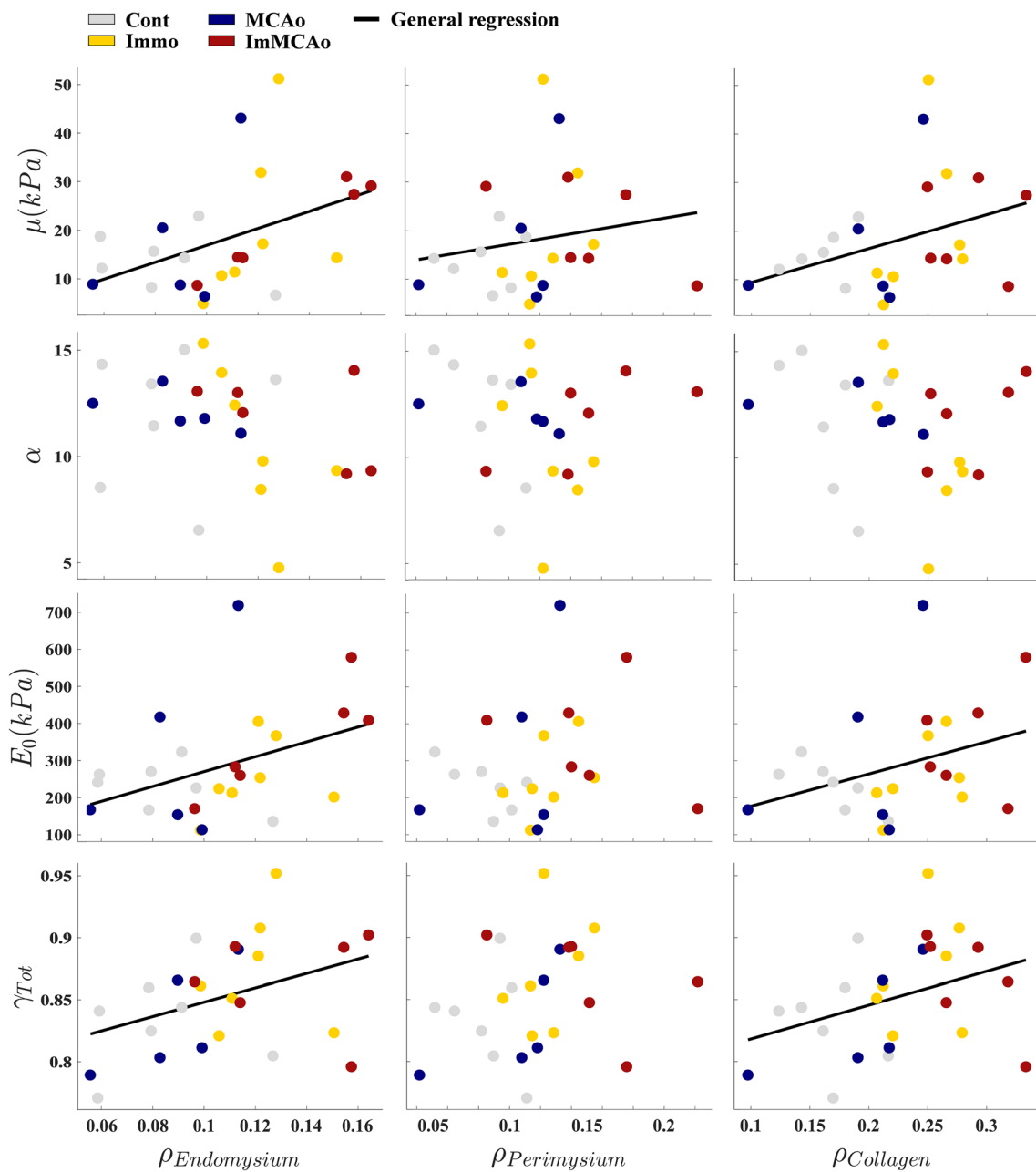


Fig. 6 Pearson correlations for all groups, immobilized groups and non-immobilized groups considered independently. Correlation between identified mechanical parameters (μ , α , E_0 , γ_T) and collagen

densities in endomysium and perimysium and total slice. Pearson coefficients (r , p) were indicated in Table 2. Trend lines were added for all groups with $p < 0.1$

surprising to find there was no significant variation after 14 days of immobilization. Change at the mRNA (messenger ribonucleic acid) and protein level occurred in the first few days (Stevens et al. 2004, 1999). During the first days, we noticed hybrid fibers with a nonsignificant increase in area density f_{I-II_a} (Fig. 1h) ($p_{Im/Cont} = 0.055$; $p_{AVC/Cont} = 0.125$ and $p_{AVC/Cont} = 0.377$).

4.6 Mechanical properties

For the mechanical study, a first-order Ogden model coupled with a second-order Maxwell model for incompressible tissues was implemented. The model accurately fits experimental data ($r^2 = 0.99 \pm 0.007$ [0.96; 0.997]). The mean value of the shear modulus μ (Fig. 5a) and the curvature

Table 2 Pearson coefficients values for all groups, immobilized (I) groups and non-immobilized (NI) groups considered independently. Correlation between identified mechanical parameters (μ , α , E_0 , γ_T) and collagen densities in endomysium and perimysium and total slice

	r	p	r_{NI}	p_{NI}	r_I	p_I
μ						
Endomysium	0.446	0.025	0.226	0.480	0.552	0.051
Perimysium	0.178	0.396	0.389	0.211	-0.126	0.681
Total collagen	0.348	0.088	0.375	0.230	0.220	0.469
α						
Endomysium	-0.291	0.158	-0.002	0.995	-0.435	0.138
Perimysium	-0.117	0.578	-0.394	0.206	0.191	0.533
Total collagen	-0.228	0.274	-0.263	0.408	-0.089	0.773
E_0						
Endomysium	0.412	0.041	0.212	0.508	0.733	0.004
Perimysium	0.202	0.332	0.286	0.367	0.059	0.849
Total collagen	0.347	0.089	0.299	0.345	0.503	0.079
γ_T						
Endomysium	0.394	0.052	0.396	0.203	-0.005	0.988
Perimysium	0.237	0.254	0.250	0.433	-0.177	0.563
Total collagen	0.360	0.077	0.369	0.238	-0.167	0.585

parameter α (Fig. 5b), respectively, ranged from 14 to 20 kPa and from 10.6 to 12.1 among groups. These values were in agreement with the literature on skeletal muscle ($\mu = 15.6 \pm 5.4$ kPa et $\alpha = 21.4 \pm 5.7$) (Bosboom et al. 2001). The Young's modulus E_0 (Fig. 5c) averaging 232 kPa for the control group lied within the range in the literature. Indeed, E_0 varied between 53 kPa (Wheatley et al. 2016a), 137 kPa (Gras et al. 2012) up to 276 kPa (Myers et al. 1998). Concerning the viscoelastic parameters, the averages of the relaxation times τ_1 and τ_2 were 5.3 and 120 s, respectively, while the averages of the relaxation coefficient γ_1 and γ_2 were 0.58 and 0.26 (Fig. 5d–g). The stresses decreased more and with a faster rate than in the work of Gras et al. (2013) ($\tau_1 = 18$ s; $\tau_2 = 395$ s; $\gamma_1 = 0.20$; $\gamma_2 = 0.19$), but decreased with a smaller amplitude and at a slower rate than in Wheatley et al. (2016a) ($\tau_1 = 0.202$ s; $\tau_2 = 12.2$ s; $\tau_3 = 262$ s; $\gamma_1 = 0.641$; $\gamma_2 = 0.124$; $\gamma_3 = 0.114$). However, the tests performed by some studies in the literature were, respectively, implemented at a rate of at $0.1\%L_0 s^{-1}$ and $17\%L_0 s^{-1}$, while muscles were stimulated at $0.5\%L_0 s^{-1}$ in the presented study. Thus, considering that viscoelastic behavior can widely vary with respect to the strain rate (Van Loocke et al. 2008), the specimen tested by Wheatley et al. (2016a) relaxed with a higher and faster rate than our tested muscle tissues. Our samples decreased with a higher and faster rate than Gras et al. (2013) specimens. Note that we did not find any significant difference in the visco-hyperelastic parameters among

the different tested groups. Nevertheless, the mean instantaneous Young's modulus E_0 of Immo MCAo and ImMCAo samples was higher than for the control group. Furthermore, we noted an increase in the shear modulus μ and a slight decrease for the curvature parameter α in the immobilized group with respect to the control and MCAo group. On the other hand, immobilization tended to produce an increase in the total relaxation ratio γ_T (Fig. 5h) in a nearly significant way ($p_{Im}^{\gamma_T} = 0.055$). Immobilized muscles, therefore, tended to become stiffer and more relaxed. Studies by others on immobilized rats show that muscle fiber (Udaka et al. 2008) and whole muscle (Honda et al. 2018) that had been immobilized in short position exhibited a significantly stiffer behavior than the control muscle group. Furthermore, studies on spastic paresis patients showed that the mechanical behavior of muscle fiber did not differ from control subjects, while injured fascicule mechanical behavior was significantly stiffer than control fascicules (de Bruin et al. 2014; Smith et al. 2011). This suggested that stiffening of skeletal muscle could be due to alteration of the extracellular matrix.

4.7 Correlation between mechanical properties and collagen densities

Correlations between mechanical parameters and collagen densities are shown in Table 2. The tensile tests and histological quantifications were implemented on different

muscles: BB and FCU, respectively. Nevertheless, on the one hand, it had been shown that BB (Lee et al. 2015; Pontén and Stål 2007) and FCU (de Bruin et al. 2014; Lieber and Fridén 2002; Yaşar et al. 2016) was affected by spastic paresis. On the other hand, BB and FCU were both flexor muscles that had been immobilized in short position in the acute phase post-stroke. Therefore, we assumed that the mechanical behaviors and the structures of both muscles were altered in the same manner. We noted that an increase in collagen density (and particularly in endomysium) was significantly correlated with an increase in muscle stiffness ($r^{E_0} = 0.412$; $p^{E_0} = 0.041$ and $r^\mu = 0.446$; $p^\mu = 0.025$). These results were in agreement with a previous study (Honda et al. 2018) and suggested that ECM alteration caused changes in the mechanical behavior. In addition, we also showed that endomysium collagen density was significantly correlated with γ_T ($r^{\gamma_T} = 0.394$; $p^{\gamma_T} = 0.052$) and tended to be negatively correlated to α ($r^\alpha = -0.291$; $p^\alpha = 0.158$). These correlations could be explained by the fact that collagen exhibited a visco-hyperelastic behavior (Yang et al. 2012) and was mainly responsible for the nonlinear behavior of skeletal muscle (Meyer and Lieber 2011). There were no in vitro studies that could be found, to the authors' knowledge, that had analyzed viscoelastic or visco-hyperelastic behavior of skeletal muscle affected by stroke or immobilization in clinical or animal studies.

Thus, we showed that immobilization in short position was more deleterious than a stroke, in particular in terms of muscle fiber atrophy, extracellular matrix thickening and mechanical behavior alteration. Rats subjected to MCAo exhibited only a little or no mechanical and structural parameter changes while immobilized rats, with or without stroke, displayed marked atrophy of skeletal muscle, fibrosis of the extracellular matrix and a tendency to visco-hyperelastic parameter changes. These results supported the hypothesis that immobilization was the starting point of a cascade of reactions within the muscle. Rats of ImMCAo group, combining stroke and immobilization of paretic forelimb was almost always the group with the worst parameters change. These alterations were similar to alterations that have been observed in patient with spastic paresis, at collagen density level (de Bruin et al. 2014) or in muscle fiber cross-sectional area (Booth et al. 2001; Pontén et al. 2007; Zogby et al. 2017) or even alterations of the mechanical behavior (Smith et al. 2011). These results suggested that the ImMCAo group represented a reliable model of spastic myopathy

post-stroke. Correlations found in the analyses revealed that the collagen amount affects the muscle mechanical behavior. Nevertheless, Pearson's linear correlation coefficients did not exceed 0.4 in absolute terms. As a result, the increase in collagen densities alone did not explain changes in the visco-hyperelastic behavior. It could be interesting to describe possible changes of titin protein or three dimensions collagen structure since they were reported as partly responsible for the mechanical behavior (Prado et al. 2005; Gillies et al. 2017) and affected by immobilization of the muscle in short position (Järvinen et al. 2002; Okita et al. 2004; Udaka et al. 2008). Lastly, we did not observe the correlation between the mechanical properties and the collagen densities were more pronounced for the endomysium collagen densities. To our knowledge, these results were not discussed in the literature and required more studies on the collagen structure in order to understand the causes of this relationship.

5 Limitations

In this work, several limitations appeared to investigate the effect of immobilization on structural and mechanical properties of skeletal muscle post-stroke. First, although rat models were reported to be reliable models of ischemic stroke (Fluri et al. 2015; Yamori et al. 1976) and of skeletal muscle injuries (Gregory et al. 2003; Strata et al. 2004; Ye et al. 2013), we noted some differences between rat and human skeletal muscles that could lead to inaccurate extrapolation (Gregory et al. 2003). In that respect, a similar study on patient post-stroke should be developed as well as other studies with other animals commonly used in skeletal muscles studies such as rabbit (Böl et al. 2012; Abraham et al. 2013; Wheatley et al. 2016b) and pigs (Van Loocke et al. 2008; Jalal and Zidi 2018). Furthermore, the short experimental duration of 14 days and the long half-life of myosin heavy chain (MHC) of 13 days (Leeuw and Pette 1996) induced no significant difference in muscle fiber typology that could be detected by immunohistology between groups. Other techniques as RT-PCR or electrophoresis could allow the measurement of RNA and MHC changes (Stevens et al. 1999). In addition, future studies should examine other microconstituents such as laminin (Townsend et al. 2016), different types of collagen (Urso et al. 2006; Honda et al. 2015) or PAX7⁺ satellite cells (Dirks et al. 2014; Kneppers et al. 2018). In this context, the degree of anisotropy change of skeletal muscle subjected to stroke and/or should be investigated. For that, an inverse finite element modeling to identify the

material parameters of an anisotropic model would be necessary. It also appears interesting to follow these alterations as well as mechanical and locomotor behaviors changes during the first days after stroke. In that sense, a longitudinal study that allowed the measurements of these changes depending on immobilization duration is currently ongoing.

6 Conclusion

The characterization and modeling of skeletal muscle confirmed on a rat model of spastic myopathy that immobilization was a deleterious factor in general and particularly following stroke. The combination of stroke and immobilization of paretic forelimb led to structural and mechanical alterations of muscle immobilized in short position. The collagen densities in connective tissue, as well as the cross-sectional area of muscle fiber, were particularly impacted by immobilization. The visco-hyperelastic mechanical behavior was also affected by the pathology. Thus, injured muscle tended to become stiffer with a more linear behavior and a larger viscous component. These results in agreement with the literature data on patients with spastic paresis suggested that our model combining stroke and immobilization was a reliable model for the study of spastic myopathy post-stroke. Further studies on animal model and on human post-stroke will make it possible to better understand the evolution of the pathology during the first weeks following a stroke. The effects determined on the animal model raised the question of the patient management following a stroke. Indeed, if our findings were to be confirmed in human, it would then be essential to modify therapeutic strategies in order to prevent the immobilization of some muscle in short position and consequently to avoid the cascade of reactions within the muscle leading to spastic myopathy. To our knowledge, this was the first time that the mechanical and structural changes of skeletal muscle that had been subjected to a stroke and/or immobilization were investigated in this manner.

Acknowledgements This work was supported by University Paris-Est Créteil. The authors would like to thank Cécile Lecoïnte and Richard

Souktani (technical surgical platform of the small animal, IMRB, University Paris-Est Créteil), HistIm platform of Cochin Institute (Paris) for histochemical and immunofluorescence staining. Primaries antibodies (BA-F8) and (SC-71) were obtained from DSHB (University of Iowa, USA).

Compliance with ethical standards

Conflict of interest All authors declare that they have no conflict of interest.

Appendix

See Fig. 7.

The model was done under isoflurane anesthesia (5% for induction, 2.25–2.5% for maintenance via artificial ventilation in 30% oxygen and 70% nitrous oxide at 1 L/min). Surgical procedures were carried out as previously described (Ouk et al. 2009). First, having exposed the right carotid, it consists of ligating pterygopalatine, common carotid and

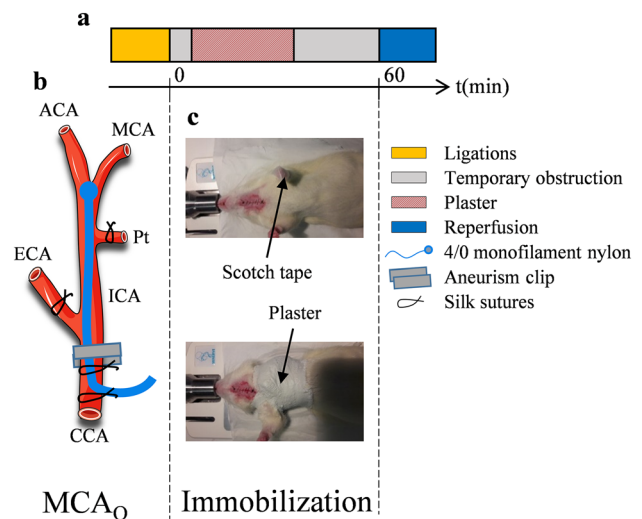


Fig. 7 **a** Diagram, **b** schema and **c** photos illustrating the methods for carrying out MCAo and immobilization. ACA, anterior cerebral artery; MCA, middle cerebral artery; Pt, pterygo-palatine artery; ECA, external carotid artery; ICA, internal carotid artery; CCA, common carotid artery

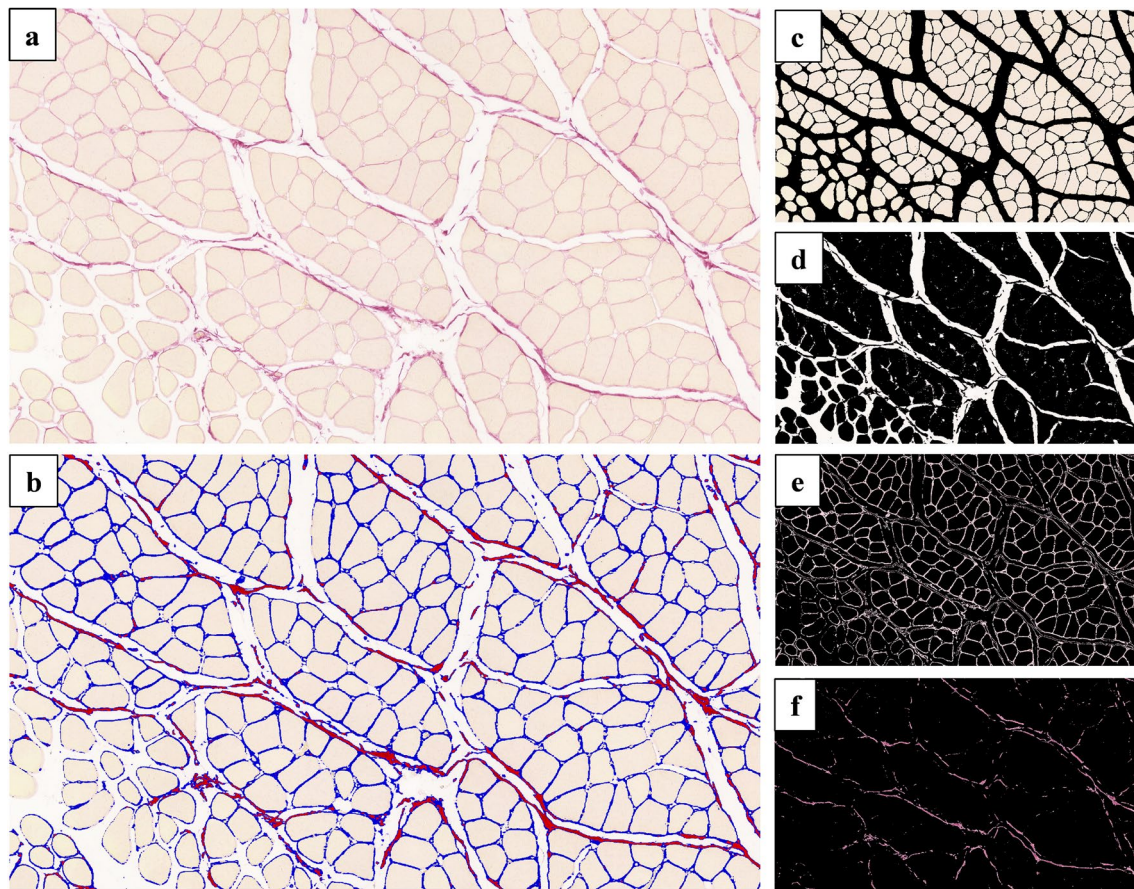


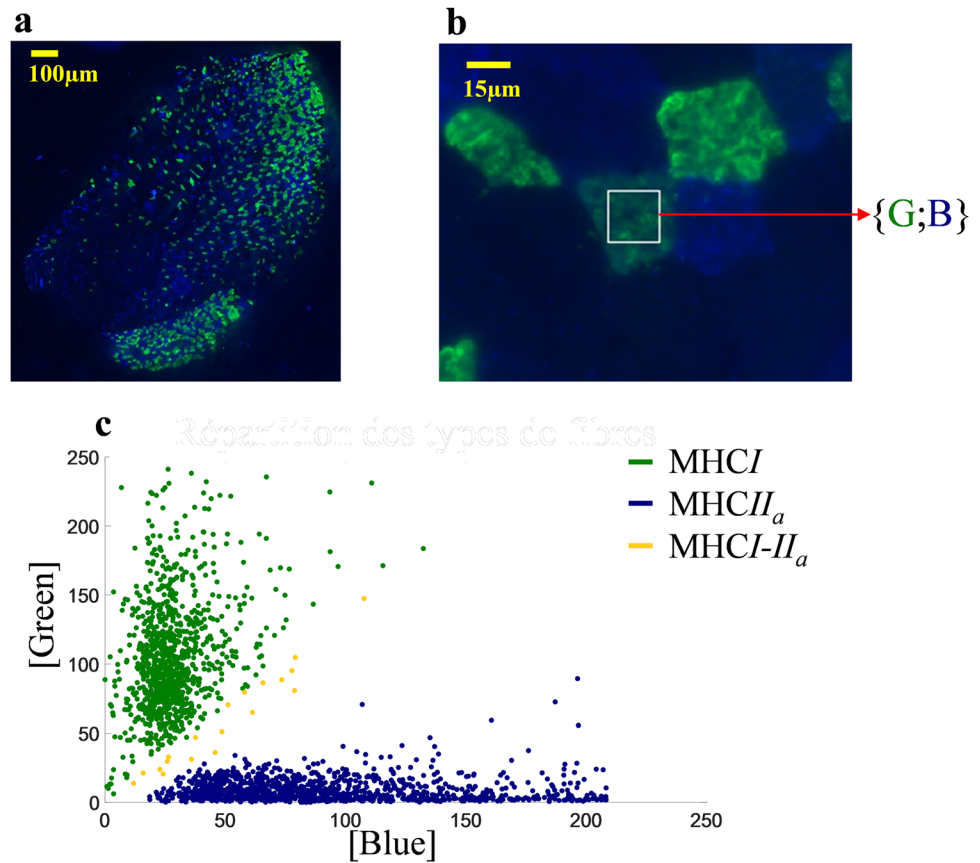
Fig. 8 Illustration of the semiautomatic collagen analysis. **a** Initial part of red Sirius slice. **b** Analyzed slice from k -mean clustering ($k=4$) with endomysium in blue and perimysium in red. **c** Cluster including muscle fiber. **d** Cluster including white background. **e** Cluster including endomysium **f** Cluster including perimysium. In order

to illustrate the process, the endomysium and perimysium cluster was colored in blue and red, respectively. Some misallocations remain after first step (k -mean clustering). That is to say endomysium in perimysium cluster and vice versa. There were manually corrected by the user with a polygonal tool

external carotid arteries with silk sutures. Then, a temporary knot and an aneurismal clip were placed successively downstream of the puncture site on the common carotid artery. A 4/0 monofilament nylon was introduced through the right common carotid artery. Once filament got to the aneurysm clip, the knot was tightened and the clip was removed. Finally, the monofilament was gently advanced of almost

20–22 mm into the internal carotid artery until resistance is felt, meaning that the rounded head of monofilament reached the middle cerebral artery. The monofilament rounded head was obtained by burning the filament end and optimized for a diameter of. After 60 min, the monofilament was removed until the rounded head was blocked by the ligature. All the silk sutures and the monofilament were left in place. Note

Fig. 9 Illustration of the semiautomatic immunohistology analysis. **a** Cross section incubated in primary antibody collagen against MHC I and MHC II. **b** Slice subdivision with selected region of interest (ROI) of one myofiber. Each myofiber was selected and a mean {Green;Blue} doublet was computed inside each ROI. **c** Myofiber automatically assigning using a *K*-mean clustering ($k=3$)



that body temperature was maintained at by a heated surgery table. The recovering place is a controlled room at 27° with an oxygen adjunction. Then, once awake, rats were placed in a cage at ambient temperature with the possibility to eat and drink ad libitum. It should be underlined that the control operation (for control and immobilized groups) consists in 60-min anesthesia and same handling without advance the monofilament until the obstruction.

See Figs. 8, 9, 10 and 11.

Whether it is for all groups (black solid line), for immobilized group (orange dotted line) or non-immobilized group (blue dotted line), we observe a strong correlation between biceps brachii wet weight and body weight (Fig. 8a). Furthermore, we show that muscle weight and cerebral infarct size are negatively correlated as previously described by Parkkinen et al. (2013) (Fig. 8b).

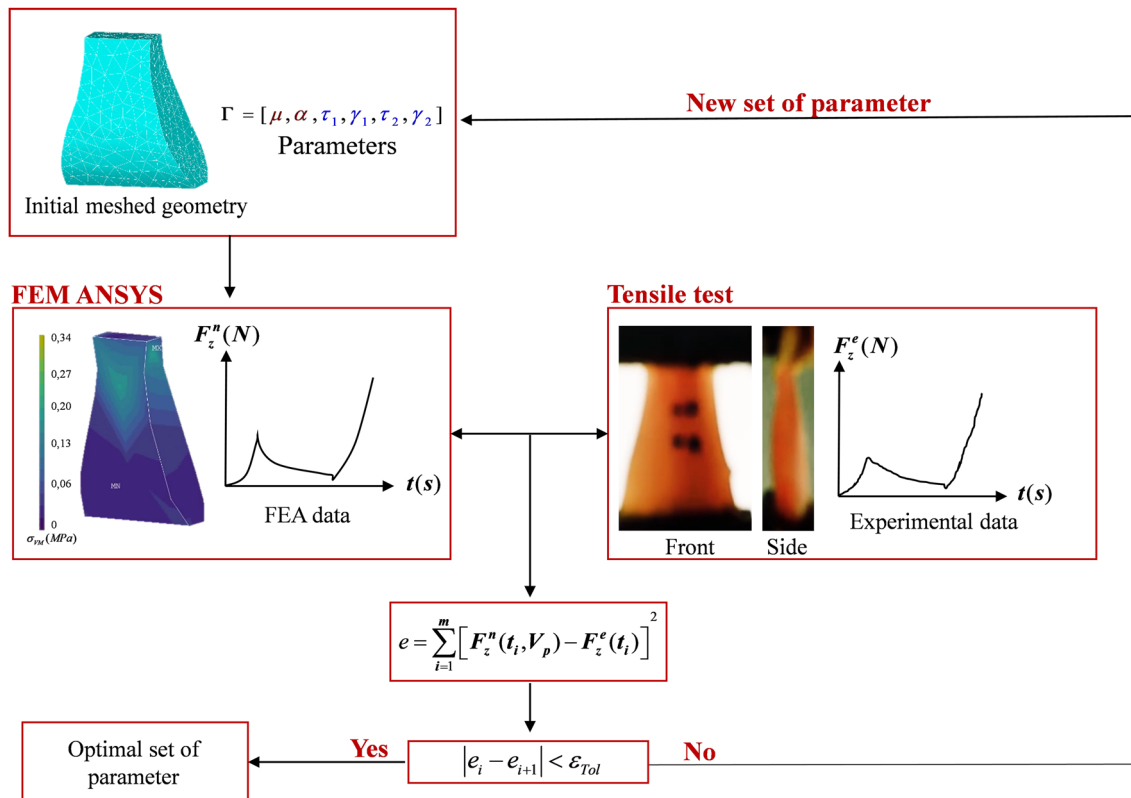
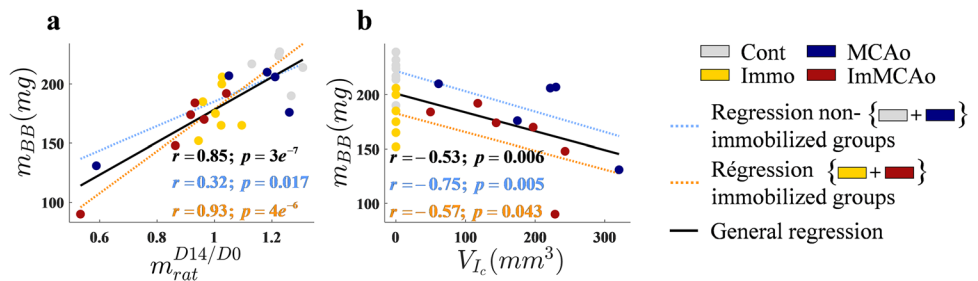


Fig. 10 Diagram of the inverse finite element method

Fig. 11 **a** Correlation between biceps brachii wet weight and body weight. **b** Correlation between muscle wet weight and cerebral infarct volume. Pearson coefficient (r , p) was indicated for all groups (black), for immobilized group (orange) or non-immobilized group (blue)



References

Abo M, Miyano S, Eun SS, Yamauchi H (2004) Histochemical characterization of skeletal muscles in rats with photochemically-induced stroke. *Brain Inj* 18:1017–1024. <https://doi.org/10.1080/02699050410001672305>

Abraham AC, Kaufman KR, Donahue TLH (2013) Phenomenological consequences of sectioning and bathing on passive muscle mechanics of the New Zealand white rabbit tibialis anterior. *J Mech Behav Biomed Mater* 17:290–295. <https://doi.org/10.1016/j.jmbbm.2012.10.003>

Bloemberg D, Quadrilatero J (2012) Rapid determination of myosin heavy chain expression in rat, mouse, and human skeletal muscle using multicolor immunofluorescence analysis. *PLoS ONE* 7:e35273. <https://doi.org/10.1371/journal.pone.0035273>

Böl M, Kruse R, Ehret AE et al (2012) Compressive properties of passive skeletal muscle—the impact of precise sample geometry on parameter identification in inverse finite element analysis. *J Biomech* 45:2673–2679. <https://doi.org/10.1016/j.jbiomech.2012.08.023>

Böl M, Ehret AE, Leichsenring K et al (2014) On the anisotropy of skeletal muscle tissue under compression. *Acta Biomater* 10:3225–3234. <https://doi.org/10.1016/j.actbio.2014.03.003>

Booth FW, Kelso JR (1973) Effect of hind-limb immobilization on contractile and histochemical properties of skeletal muscle. *Pflügers Arch* 342:231–238

Booth CM, Cortina-Borja MJ, Theologis TN (2001) Collagen accumulation in muscles of children with cerebral palsy and correlation with severity of spasticity. *Dev Med Child Neurol* 43:314–320

Bosboom EMH, Hesselink MKC, Oomens CWJ et al (2001) Passive transverse mechanical properties of skeletal muscle under in vivo

- compression. *J Biomech* 34:1365–1368. [https://doi.org/10.1016/S0021-9290\(01\)00083-5](https://doi.org/10.1016/S0021-9290(01)00083-5)
- Bouley J, Fisher M, Henninger N (2007) Comparison between coated vs. uncoated suture middle cerebral artery occlusion in the rat as assessed by perfusion/diffusion weighted imaging. *Neurosci Lett* 412:185–190. <https://doi.org/10.1016/j.neulet.2006.11.003>
- Calvo B, Ramírez A, Alonso A et al (2010) Passive nonlinear elastic behaviour of skeletal muscle: experimental results and model formulation. *J Biomech* 43:318–325. <https://doi.org/10.1016/j.jbiomech.2009.08.032>
- Chapman MA, Pichika R, Lieber RL (2015) Collagen crosslinking does not dictate stiffness in a transgenic mouse model of skeletal muscle fibrosis. *J Biomech* 48:375–378. <https://doi.org/10.1016/j.jbiomech.2014.12.005>
- Chawla A, Mukherjee S, Karthikeyan B (2009) Characterization of human passive muscles for impact loads using genetic algorithm and inverse finite element methods. *Biomech Model Mechanobiol* 8:67–76. <https://doi.org/10.1007/s10237-008-0121-6>
- Cheung DK, Climans SA, Black SE et al (2016) Lesion characteristics of individuals with upper limb spasticity after stroke. *Neurorehabil Neural Repair* 30:63–70. <https://doi.org/10.1177/1545968315585357>
- Coq JO, Xerri C (1999) Tactile impoverishment and sensorimotor restriction deteriorate the forepaw cutaneous map in the primary somatosensory cortex of adult rats. *Exp Brain Res* 129:518–531
- de Bruin M, Smeulders MJ, Kreulen M et al (2014) Intramuscular connective tissue differences in spastic and control muscle: a mechanical and histological study. *PLoS ONE* 9:e101038. <https://doi.org/10.1371/journal.pone.0101038>
- De Deyne PG, Hafer-Macko CE, Ivey FM et al (2004) Muscle molecular phenotype after stroke is associated with gait speed. *Muscle Nerve* 30:209–215. <https://doi.org/10.1002/mus.20085>
- Desgeorges MM, Devillard X, Toutain J et al (2017) Pharmacological inhibition of myostatin improves skeletal muscle mass and function in a mouse model of stroke. *Sci Rep*. <https://doi.org/10.1038/s41598-017-13912-0>
- Dirks ML, Wall BT, Snijders T et al (2014) Neuromuscular electrical stimulation prevents muscle disuse atrophy during leg immobilization in humans. *Acta Physiol Oxf Engl* 210:628–641. <https://doi.org/10.1111/apha.12200>
- Fluri F, Schuhmann MK, Kleinschnitz C (2015) Animal models of ischemic stroke and their application in clinical research. *Drug Des Dev Ther* 9:3445–3454. <https://doi.org/10.2147/DDDT.S56071>
- Gautier S, Ouk T, Petraut O et al (2009) Neutrophils contribute to intracerebral haemorrhages after treatment with recombinant tissue plasminogen activator following cerebral ischaemia. *Br J Pharmacol* 156:673–679. <https://doi.org/10.1111/j.1476-5381.2009.00068.x>
- Ghoreishy MHR (2012) Determination of the parameters of the Prony series in hyper-viscoelastic material models using the finite element method. *Mater Des* 35:791–797. <https://doi.org/10.1016/j.matdes.2011.05.057>
- Gillies AR, Chapman MA, Bushong EA et al (2017) High resolution three-dimensional reconstruction of fibrotic skeletal muscle extracellular matrix. *J Physiol* 595:1159–1171. <https://doi.org/10.1113/JP273376>
- Gracies J-M (2005) Pathophysiology of spastic paresis. II: Emergence of muscle overactivity. *Muscle Nerve* 31:552–571. <https://doi.org/10.1002/mus.20285>
- Gracies J-M (2015) Coefficients of impairment in deforming spastic paresis. *Ann Phys Rehabil Med* 58:173–178. <https://doi.org/10.1016/j.rehab.2015.04.004>
- Gras L-L, Mitton D, Viot P, Laporte S (2012) Hyper-elastic properties of the human sternocleidomastoideus muscle in tension. *J Mech Behav Biomed Mater* 15:131–140. <https://doi.org/10.1016/j.jmbbm.2012.06.013>
- Gras L-L, Mitton D, Viot P, Laporte S (2013) Viscoelastic properties of the human sternocleidomastoideus muscle of aged women in relaxation. *J Mech Behav Biomed Mater* 27:77–83. <https://doi.org/10.1016/j.jmbbm.2013.06.010>
- Gregory CM, Vandenborne K, Castro MJ, Dudley GA (2003) Human and rat skeletal muscle adaptations to spinal cord injury. *Can J Appl Physiol Rev Can Physiol Appl* 28:491–500
- Hafer-Macko CE, Ryan AS, Ivey FM, Macko RF (2008) Skeletal muscle changes after hemiparetic stroke and potential beneficial effects of exercise intervention strategies. *J Rehabil Res Dev* 45:261–272
- Holzapfel GA (1996) On large strain viscoelasticity: continuum formulation and finite element applications to elastomeric structures. *Int J Numer Methods Eng* 39:3903–3926. [https://doi.org/10.1002/\(SICI\)1097-0207\(19961130\)39:22%3c3903:AID-NME34%3e3.0.CO;2-C](https://doi.org/10.1002/(SICI)1097-0207(19961130)39:22%3c3903:AID-NME34%3e3.0.CO;2-C)
- Honda Y, Sakamoto J, Nakano J et al (2015) Upregulation of interleukin-1 β /transforming growth factor- β 1 and hypoxia relate to molecular mechanisms underlying immobilization-induced muscle contracture. *Muscle Nerve* 52:419–427. <https://doi.org/10.1002/mus.24558>
- Honda Y, Tanaka M, Tanaka N et al (2018) Relationship between extensibility and collagen expression in immobilized rat skeletal muscle. *Muscle Nerve* 57:672–678. <https://doi.org/10.1002/mus.26011>
- Jalal N, Zidi M (2018) Effect of cryopreservation at -80°C on visco-hyperelastic properties of skeletal muscle tissue. *J Mech Behav Biomed Mater* 77:572–577. <https://doi.org/10.1016/j.jmbbm.2017.10.006>
- Järvinen TAH, Józsa L, Kannus P et al (2002) Organization and distribution of intramuscular connective tissue in normal and immobilized skeletal muscles. An immunohistochemical, polarization and scanning electron microscopic study. *J Muscle Res Cell Motil* 23:245–254
- Jones TA, Schallert T (1994) Use-dependent growth of pyramidal neurons after neocortical damage. *J Neurosci Off J Soc Neurosci* 14:2140–2152
- Junqueira LC, Bignolas G, Brentani RR (1979) Picrosirius staining plus polarization microscopy, a specific method for collagen detection in tissue sections. *Histochem J* 11:447–455
- Kneppers A, Leermakers P, Pansters N et al (2018) Coordinated regulation of skeletal muscle mass and metabolic plasticity during recovery from disuse. *FASEB J*. <https://doi.org/10.1096/fj.201701403RRR>
- Lee SSM, Spear S, Rymer WZ (2015) Quantifying changes in material properties of stroke-impaired muscle. *Clin Biomech* 30:269–275. <https://doi.org/10.1016/j.clinbiomech.2015.01.004>
- Leeuw T, Pette D (1996) Coordinate changes of myosin light and heavy chain isoforms during forced fiber type transitions in rabbit muscle. *Dev Genet* 19:163–168. [https://doi.org/10.1002/\(SICI\)1520-6408\(1996\)19:2%3c163:AID-DVG8%3e3.0.CO;2-7](https://doi.org/10.1002/(SICI)1520-6408(1996)19:2%3c163:AID-DVG8%3e3.0.CO;2-7)
- Li L, Rong W, Ke Z et al (2011) Muscle activation changes during body weight support treadmill training after focal cortical ischemia: a rat hindlimb model. *J Electromyogr Kinesiol Off J Int Soc Electrophysiol Kinesiol* 21:318–326. <https://doi.org/10.1016/j.jelekin.2010.09.008>
- Lieber RL, Fridén J (2002) Spasticity causes a fundamental rearrangement of muscle-joint interaction. *Muscle Nerve* 25:265–270
- Liu Y, Zhao Y, Huang F et al (2016) Combination of early constraint-induced movement therapy and fasudil enhances motor recovery after ischemic stroke in rats. *Int J Neurosci* 126:168–173. <https://doi.org/10.3109/00207454.2014.998759>

- Longa EZ, Weinstein PR, Carlson S, Cummins R (1989) Reversible middle cerebral artery occlusion without craniectomy in rats. *Stroke J Cereb Circ* 20:84–91
- Meyer GA, Lieber RL (2011) Elucidation of extracellular matrix mechanics from muscle fibers and fiber bundles. *J Biomech* 44:771–773. <https://doi.org/10.1016/j.jbiomech.2010.10.044>
- Mohammadkhan M, Murphy P, Simms CK (2016) The in vitro passive elastic response of chicken pectoralis muscle to applied tensile and compressive deformation. *J Mech Behav Biomed Mater* 62:468–480. <https://doi.org/10.1016/j.jmbbm.2016.05.021>
- Myers BS, Woolley CT, Slotter TL et al (1998) The influence of strain rate on the passive and stimulated engineering stress–large strain behavior of the rabbit tibialis anterior muscle. *J Biomech Eng* 120:126–132
- Norvang OP, Hokstad A, Taraldsen K, et al (2018) Time spent lying, sitting, and upright during hospitalization after stroke: a prospective observation study. *BMC Neurol* 18:138. <https://doi.org/10.1186/s12883-018-1134-0>
- Okita M, Yoshimura T, Nakano J et al (2004) Effects of reduced joint mobility on sarcomere length, collagen fibril arrangement in the endomysium, and hyaluronan in rat soleus muscle. *J Muscle Res Cell Motil* 25:159–166
- Ouk T (2009) Ischémie cérébrale et interactions leucocyte-endothélium : modulation pharmacologique par les récepteurs nucléaires PPARs. Lille 2
- Ouk T, Laprais M, Bastide M et al (2009) Withdrawal of fenofibrate treatment partially abrogates preventive neuroprotection in stroke via loss of vascular protection. *Vasc Pharmacol* 51:323–330. <https://doi.org/10.1016/j.vph.2009.08.002>
- Parkkinen S, Ortega FJ, Kuptsova K et al (2013) Gait impairment in a rat model of focal cerebral ischemia. *Stroke Res Treat* 2013:410972. <https://doi.org/10.1155/2013/410972>
- Picelli A, Tamburin S, Gajofatto F et al (2014) Association between severe upper limb spasticity and brain lesion location in stroke patients. *Biomed Res Int* 2014:e162754. <https://doi.org/10.1155/2014/162754>
- Pontén EM, Stål PS (2007) Decreased capillarization and a shift to fast myosin heavy chain IIX in the biceps brachii muscle from young adults with spastic paresis. *J Neurol Sci* 253:25–33. <https://doi.org/10.1016/j.jns.2006.11.006>
- Pontén E, Gantelius S, Lieber RL (2007) Intraoperative muscle measurements reveal a relationship between contracture formation and muscle remodeling. *Muscle Nerve* 36:47–54. <https://doi.org/10.1002/mus.20780>
- Prado LG, Makarenko I, Andresen C et al (2005) Isoform diversity of giant proteins in relation to passive and active contractile properties of rabbit skeletal muscles. *J Gen Physiol* 126:461–480. <https://doi.org/10.1085/jgp.200509364>
- Rogers DC, Campbell CA, Stretton JL, Mackay KB (1997) Correlation between motor impairment and infarct volume after permanent and transient middle cerebral artery occlusion in the rat. *Stroke* 28:2060–2066. <https://doi.org/10.1161/01.STR.28.10.2060>
- Schipke J, Brandenberger C, Rajces A et al (2017) Assessment of cardiac fibrosis: a morphometric method comparison for collagen quantification. *J Appl Physiol Bethesda Md* 1985 122:1019–1030. <https://doi.org/10.1152/jappphysiol.00987.2016>
- Shortland AP, Harris CA, Gough M, Robinson RO (2002) Architecture of the medial gastrocnemius in children with spastic diplegia. *Dev Med Child Neurol* 44:158–163
- Smith LR, Barton ER (2014) Collagen content does not alter the passive mechanical properties of fibrotic skeletal muscle in mdx mice. *Am J Physiol Cell Physiol* 306:C889–898. <https://doi.org/10.1152/ajpcell.00383.2013>
- Smith LR, Lee KS, Ward SR et al (2011) Hamstring contractures in children with spastic cerebral palsy result from a stiffer extracellular matrix and increased in vivo sarcomere length. *J Physiol* 589:2625–2639. <https://doi.org/10.1113/jphysiol.2010.203364>
- Spector SA, Simard CP, Fournier M et al (1982) Architectural alterations of rat hind-limb skeletal muscles immobilized at different lengths. *Exp Neurol* 76:94–110. [https://doi.org/10.1016/0014-4886\(82\)90104-2](https://doi.org/10.1016/0014-4886(82)90104-2)
- Stevens L, Sultan KR, Peuker H et al (1999) Time-dependent changes in myosin chain mRNA and protein isoforms in unloaded soleus muscles of rat. *Am J Physiol* 277(6 Pt 1):C1122–C1129
- Stevens L, Bastide B, Bozzo C, Mounier Y (2004) Hybrid fibres under slow-to-fast transformations: expression is of myosin heavy and light chains in rat soleus muscle. *Pflüg Arch* 448:507–514. <https://doi.org/10.1007/s00424-004-1287-0>
- Strata F, Coq J-O, Byl N, Merzenich MM (2004) Effects of sensorimotor restriction and anoxia on gait and motor cortex organization: implications for a rodent model of cerebral palsy. *Neuroscience* 129:141–156. <https://doi.org/10.1016/j.neuroscience.2004.07.024>
- Tabary JC, Tabary C, Tardieu C et al (1972) Physiological and structural changes in the cat's soleus muscle due to immobilization at different lengths by plaster casts*. *J Physiol* 224:231–244. <https://doi.org/10.1113/jphysiol.1972.sp009891>
- Townsend JR, Hoffman JR, Fragala MS et al (2016) A microbiopsy method for immunohistological and morphological analysis: a pilot study. *Med Sci Sports Exerc* 48:331–335. <https://doi.org/10.1249/MSS.0000000000000772>
- Udaka J, Ohmori S, Terui T et al (2008) Disuse-induced preferential loss of the giant protein titin depresses muscle performance via abnormal sarcomeric organization. *J Gen Physiol* 131:33–41. <https://doi.org/10.1085/jgp.200709888>
- Urso ML, Scrimgeour AG, Chen Y-W et al (2006) Analysis of human skeletal muscle after 48 h immobilization reveals alterations in mRNA and protein for extracellular matrix components. *J Appl Physiol Bethesda Md* 1985 101:1136–1148. <https://doi.org/10.1152/jappphysiol.00180.2006>
- Van Loocke M, Lyons CG, Simms CK (2006) A validated model of passive muscle in compression. *J Biomech* 39:2999–3009. <https://doi.org/10.1016/j.jbiomech.2005.10.016>
- Van Loocke M, Lyons CG, Simms CK (2008) Viscoelastic properties of passive skeletal muscle in compression: stress-relaxation behaviour and constitutive modelling. *J Biomech* 41:1555–1566. <https://doi.org/10.1016/j.jbiomech.2008.02.007>
- Wheatley BB, Morrow DA, Odegard GM et al (2016a) Skeletal muscle tensile strain dependence: hyperviscoelastic nonlinearity. *J Mech Behav Biomed Mater* 53:445–454. <https://doi.org/10.1016/j.jmbbm.2015.08.041>
- Wheatley BB, Odegard GM, Kaufman KR, Donahue TLH (2016b) How does tissue preparation affect skeletal muscle transverse isotropy? *J Biomech*. <https://doi.org/10.1016/j.jbiomech.2016.06.034>
- Williams PE, Goldspink G (1984) Connective tissue changes in immobilised muscle. *J Anat* 138:343–350
- Yamori Y, Horie R, Handa H et al (1976) Pathogenetic similarity of strokes in stroke-prone spontaneously hypertensive rats and humans. *Stroke* 7:46–53
- Yang L, van der Werf KO, Dijkstra PJ et al (2012) Micromechanical analysis of native and cross-linked collagen type I fibrils supports the existence of microfibrils. *J Mech Behav Biomed Mater* 6:148–158. <https://doi.org/10.1016/j.jmbbm.2011.11.008>
- Yaşar E, Adigüzel E, Kesikburun S et al (2016) Assessment of forearm muscle spasticity with sonoelastography in patients with stroke. *Br J Radiol* 89:20160603. <https://doi.org/10.1259/bjr.20160603>
- Ye F, Baligand C, Keener JE et al (2013) Hindlimb muscle morphology and function in a new atrophy model combining spinal cord injury and cast immobilization. *J Neurotrauma* 30:227–235. <https://doi.org/10.1089/neu.2012.2504>

- Zhang P, Zhang Q, Pu H et al (2012) Very early-initiated physical rehabilitation protects against ischemic brain injury. *Front Biosci Elite Ed* 4:2476–2489
- Zogby AM, Dayanidhi S, Chambers HG et al (2017) Skeletal muscle fiber-type specific succinate dehydrogenase activity in cerebral palsy. *Muscle Nerve* 55:122–124. <https://doi.org/10.1002/mus.25379>
- Zvejniece L, Svalbe B, Liepinsh E et al (2012) The sensorimotor and cognitive deficits in rats following 90- and 120-min transient occlusion of the middle cerebral artery. *J Neurosci Methods* 208:197–204. <https://doi.org/10.1016/j.jneumeth.2012.05.018>

Publisher's Note Springer Nature remains neutral with regard to jurisdictional claims in published maps and institutional affiliations.